Nanoscale

PAPER

View Article Online
View Journal | View Issue

Cite this: *Nanoscale*, 2025, **17**, 13275

A MPB-intensified tube microreactor system for continuous synthesis of Ag^+ doped CdS quantum dots†

Chuwei Zhu,‡ Yuxi Li,‡ Tailei Hou, Xiaole Gu, Xinyuan Li, * Le Sang * and Jiatao Zhang *

Received 17th March 2025,
Accepted 28th April 2025

DOI: 10.1039/d5nr01114k

rsc.li/nanoscale

Recent advances in microreactor technology have established these systems as promising platforms for colloidal nanocrystal synthesis. Nevertheless, the continuous production of high-quality doped quantum dots (QDs) with precise control over their optical properties continues to present significant technical challenge. This study introduces a micropacked bed (MPB) intensified tube microreactor system for the efficient and continuous synthesis of Ag^+ doped CdS QDs ($CdS:Ag^+$ doped-QDs). Through systematic optimization of reaction parameters, the MPB system achieved a photoluminescent quantum yield (PLQY) of 50.8% under optimized conditions (18 cm MPB filled with 2.0 mm glass beads, 0.2 mL min^{-1} flow rate, and 70 °C reaction temperature), and the yield increased to 64.6%. These results represent significant improvements over the traditional batch flask method (40% PLQY, 43.01% yield) and the microreactor method (43% PLQY, 48.41% yield). The developed MPB system demonstrates multiple operational advantages: reaction duration reduced to 30 minutes, simplified fluidic architecture requiring only two pumps (*vs.* three in conventional systems), and enhanced flow rate (0.2 mL min^{-1} *vs.* 40 μL min^{-1}). Production capacity analysis revealed 6-fold and 2.67-fold increases in $CdS:Ag^+$ doped-QD output compared to the batch flask method and the microreactor method, respectively, per unit time. This continuous flow strategy establishes a viable pathway for industrial-scale synthesis of doped quantum dots with enhanced process efficiency and material quality.

Introduction

Microreactors offer significant advantages over conventional reactors, including enhanced mass/heat transfer efficiency, rapid mixing kinetics, and high surface-to-volume ratios.[1–6] These characteristics enable diverse application fields in CO_2 capture,[7] hydrogen storage,[8] and nanomaterial synthesis.[9] Modern microfluidic systems integrate multifunctional modules to achieve continuous processing from reagent delivery to product collection, thereby ensuring production consistency while demonstrating industrial-scale potential.[10–12]

Quantum dots (QDs), a class of semiconductor nanomaterials, demonstrate exceptional optoelectronic performance in applications such as light-emitting diodes (LEDs), luminescent solar concentrators (LSCs), quantum dot sensitized solar cells (QDSCs), and photodetectors,[13–19] by virtue of their unique quantum size effect and surface effect.[20–28] Current synthesis methodologies primarily employ wet chemical approaches such as the cation exchange method,[29–31] the thermal injection method,[32] the sol–gel method,[33] the hydrothermal method,[34] and microwave- and ultrasonic-assisted synthesis methods.[35] Compared to pristine QDs, electronically doped QDs (Ed-QDs), normally achieved by heterovalent doping, exhibit superior fluorescence properties. At present, there are studies using $CdS:Ag^+$ doped-QDs in applications such as 3D printing anti-counterfeiting,[36,37] fluorescence sensors[38] and other fields, showing the diverse application potential of Ed-QDs. Despite some progress in atomic-level structural control, scalable production of high-quality Ed-QDs remains technically challenging, necessitating innovative synthesis strategies.[39]

Emerging research highlights microreactors as promising platforms for colloidal nanocrystal synthesis, including QDs.[29]

Beijing Key Laboratory of Construction-Tailorable Advanced Functional Materials and Green Applications, MOE Key Laboratory of Cluster Science, MIIT Key Laboratory of Medical Molecule Science and Pharmaceutical Engineering, School of Chemistry and Chemical Engineering, Beijing Institute of Technology, Beijing 100081, China. E-mail: zhangjt@bit.edu.cn, xinyuanli@bit.edu.cn, lesang@bit.edu.cn

†Electronic supplementary information (ESI) available. See DOI: https://doi.org/10.1039/d5nr01114k

‡These authors contributed equally to this work.

Their operational advantages stem from rapid reactant homogenization and precise thermal regulation, enabling controlled nanocrystal growth through optimized mass/heat transfer dynamics.[40] While our prior work demonstrated quality improvements in QDs over the batch flask method, limitations persisted regarding energy-intensive multi-pump configurations and suboptimal flow rates, which not only limit its potential for mass production but also increase energy consumption. Furthermore, a fundamental understanding of Ed-QD formation thermodynamics/kinetics requires deeper investigation.[41]

To address these challenges, we developed a MPB-intensified tube microreactor system for continuous synthesis of CdS:Ag^+ doped-QDs. Systematic parameter optimization (flow rate, temperature, and MPB length/particle size) enabled precise control over cation exchange kinetics. As a result, CdS:Ag^+ doped-QDs with higher PLQY (50.8%) and yield (64.6%) were produced in the MPB-intensified tube microreactor system, realizing more stable, controllable, and efficient synthesis of Ed-QDs. The optimized system demonstrated 6-fold and 2.67-fold production increases over the batch flask method and microreactor method, respectively, while reducing the reaction duration to 30 minutes. The MPB system simplified the fluidic architecture requiring only two pumps (*vs.* three in conventional systems) and achieved an enhanced flow rate (0.2 mL min^{-1} *vs.* 40 μL min^{-1}). This work establishes a robust framework for industrial-scale Ed-QDs synthesis through enhancing process efficiency and mechanistic control.

Experimental section

Chemicals

Oleic acid (OA, 90%, Heowns), oleyl amine (OAm, 80%–90%, Meryer), sublimed sulfur (S, CP, Xilong Scientific), tributyl phosphine (TBP, 95%, Meryer), $AgNO_3$ (AR, Xilong Scientific), toluene (AR, Fuyu Chemical), $Fe(NO_3)_3{\cdot}9H_2O$ (AR, Tong Guang), methyl alcohol (AR, Tong Guang), ethanol (AR, Tong Guang), and cadmium acetate (AR, Aladdin) were used as received without further purification.

Synthesis

Synthesis of Ag_2S QDs. Monodisperse Ag nanoparticles with a size of about 4 nm were prepared according to previous work by Wang and co-workers.[42] Typically, $AgNO_3$ (0.34 g) and $Fe(NO_3)_3{\cdot}9H_2O$ (0.08 g) were added to a mixture of OA (20 mL) and OAm (20 mL) under vigorous stirring. Then, the mixture was heated from 25 °C to 120 °C and maintained for another 60 min under N_2 flow. After cooling to room temperature, the products were collected by precipitation and centrifugation with ethanol three times and redispersed in 14 mL of toluene. 300 μL of Ag NPs and 3 mL of S precursors (prepared by the reaction of 2 mmol of S powder with 5 mL of OAm and 10 mL of OA at 120 °C for 1.5 h) were added to a single-neck flask containing 6 mL of toluene and reacted at 50 °C for 1 h. The as-prepared Ag_2S QDs were purified by precipitation with ethanol and centrifugation at 5000 rpm for 8 min and redispersed in 3 mL of toluene.

Synthesis of CdS:Ag^+ doped-QDs. The microreactor system was built with three parts of feeding, reaction, and product collection (Fig. 1). Two types of solution were introduced separately into the microreactor system *via* plunger pumps. One of the plunger pumps transferred solution A (Q_A), dispersing TBP in toluene. Another pump transferred solution B (Q_B) containing several solutions. Solution B consisted of Ag_2S QDs dispersed in toluene, $Cd(NO_3)_2{\cdot}4H_2O$ methanol solution, toluene, OA and OAm. Toluene was chosen as the solvent for its low viscosity and excellent solubility for the precursors and QDs. By adjusting the flow rate, the residence time of the solution can be easily controlled, to prepare QDs with an easily tunable reaction time. The reaction part consisted of a MPB and a tube microreactor. The MPB section was a micropacked bed made of stainless steel with glass beads that could be replaced with different internal particle sizes or reactor lengths. Its specific structure and size are shown in Fig. S1.† The tube microreactor section was a PTFE tube with an inner diameter of 1 mm, an outer diameter of 2 mm and a length of 150 cm. The two sections were connected by a junction. The fluids were then mixed in the MPB section before flowing into the reaction area and being settled in a water bath. As the reaction progressed in the tube microreactor section, the color of the solution changed from brown to bright yellow and exhibited intense fluorescence under UV light irradiation, indicating that CdS:Ag^+ doped-QDs had been successfully synthesized. The as-prepared CdS:Ag^+ doped-QDs were then precipitated by ethanol, centrifuged at 7000 rpm for 5 min, and dispersed in toluene for subsequent experiments and characterization. Specific reaction conditions are described in the ESI.†

Characterization

Low-Resolution Transmission Electron Microscopy (TEM) images were obtained by using a JEOL JEM-1200EX instrument working at 80 kV. High-Resolution Transmission Microscopy (HRTEM) images were collected by using a Talos F200X G2. X-ray diffraction (XRD) was measured by using a Bruker D8 Advance X-ray powder diffractometer. X-ray photoelectron spectroscopy (XPS) analysis was performed by using a Thermo Escalab 250XI spectrometer. The absorption spectra were recorded by using a Shimadzu UV-3600 UV-vis-NIR spectrophotometer. Photoluminescence (PL) spectra were characterized by a Hitachi F-4500 fluorescence spectrometer. A FLS1000 PL spectrometer (Edinburgh, UK) with a 450 W ozone-free xenon arc lamp as the excitation source and a PMT-900 as the signal detector were used to measure the luminescence lifetime and fluorescence quantum yield (PLQY).

Results and discussion

The continuous synthesis was realized by using a MPB with glass beads combined with a tube microreactor. The reaction mechanism for the high-quality deep-site heterovalent doped

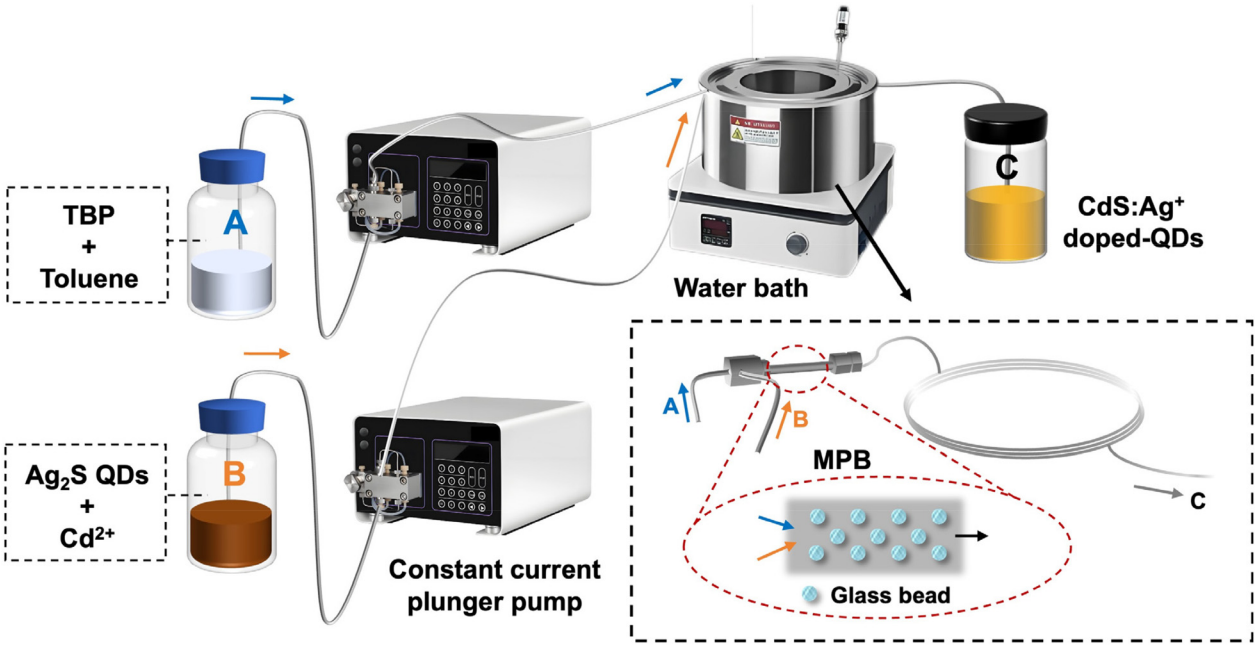

Fig. 1 Synthesis process of CdS:Ag^+ doped-QDs *via* the MPB-intensified tube microreactor system.

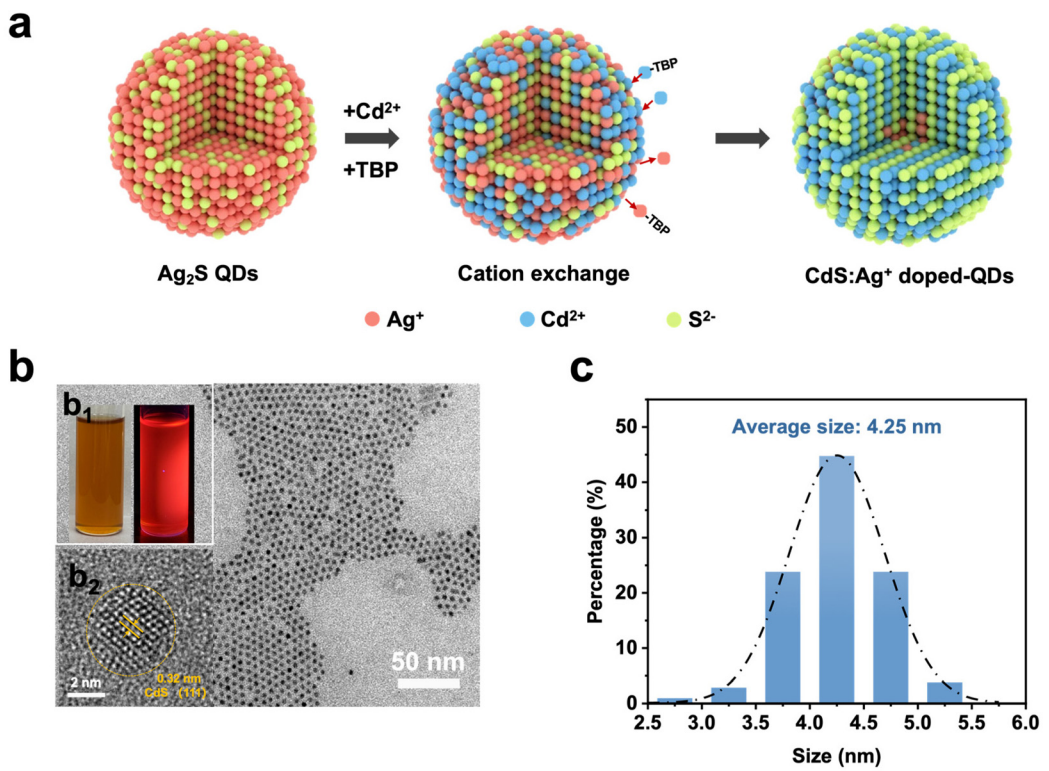

Fig. 2 (a) Schematic illustration of the synthesis strategy for CdS:Ag^+ doped-QDs. (b) TEM image of CdS:Ag^+ doped-QDs synthesized by the MPB-intensified tube microreactor system. Inset: (b_1) HRTEM image of CdS:Ag^+ doped-QDs and (b_2) optical images of CdS:Ag^+ doped-QDs under visible light and λ = 365 nm UV light irradiation. (c) Particle size analysis of CdS:Ag^+ doped-QDs synthesized by the MPB-intensified tube microreactor system.

CdS:Ag^+ QDs synthesized by cation exchange from Ag_2S QDs is illustrated in Fig. 2a. With the introduction of trace amounts of TBP, Cd^{2+} would gradually replace Ag^+ from the outside and inside of Ag_2S, forming single-crystalline CdS with a small amount of residual Ag^+ doping. The optical images of the synthesized colloidal QDs are shown in the inset of Fig. 2b_1, which shows red fluorescence under 365 nm ultraviolet light illumination. The TEM image and particle size analysis of

CdS:Ag^+ doped-QDs are shown in Fig. 2b and c. They indicate that the QDs synthesized by the MPB are highly monodispersed with an average diameter of around 4.25 nm. Compared with the CdS:Ag^+ doped-QDs prepared by the traditional batch flask method (Fig. S2a and b†), the diameter dispersion of QDs synthesized by a MPB is better and the morphology is relatively more uniform. The HRTEM image of CdS:Ag^+ doped-QDs shows clear lattice fringes as illustrated in Fig. $2b_2$ and Fig. S3,† which indicate the high crystallinity of as-prepared QDs. The lattice spacing is measured at 0.32 nm, which matches well with the (111) planes of cubic phase CdS. Table S1† shows the EDS elemental content of CdS:Ag^+ doped-QDs synthesized by the MPB system. The results prove that there are trace amounts of Ag^+ remaining within the CdS. The ICP result (Table S2†) also shows that. Besides, the XRD pattern of the CdS:Ag^+ doped-QDs prepared by MPB is characterized as shown in Fig. S4,† which could be indexed to the zinc-sphalerite structure of CdS (JCPDS no. 10-0454) and is equivalent to the XRD pattern of the batch flask method. In order to further investigate the electronic structure of CdS:Ag^+ doped-QDs prepared in batch and continuous methods, the XPS spectra of Ag, S and Cd in CdS:Ag^+ doped-QDs are characterized as shown in Fig. S5.† It can be observed that the Ag 3d orbit splits into two peaks, which could be fitted with $3d_{5/2}$ (368.0 eV) and $3d_{3/2}$ (374.0 eV). This result is consistent with the results described in the literature.[36] The XPS spectra of Cd 3d correspond to Cd $3d_{5/2}$ (405.0 eV) and Cd $3d_{3/2}$ (411.8 eV) of CdS and the XPS spectra of the S 2p orbit show two peaks at 161.4 eV and 162.5 eV, which are consistent with the XPS test results of Cd and S in CdS.[43] In addition, the symmetrical bimodal appearance of Ag 3d and Cd 3d can be interpreted as the result of orbital spin splitting, indicating that there is no significant difference in the structure of the CdS:Ag^+ doped-QDs synthesized by the two methods.

Then, the effects of different experimental conditions on the PL properties of CdS:Ag^+ doped-QDs were investigated, including reaction temperature, flow rate, concentration of TBP, and the internal particle size and length of the MPB in the continuous method. First, to explore the effects of reaction temperature and flow rate ratio on the luminescence performance of QDs, the experiments of this part were carried out without adding the MPB. Fig. 3a shows the effect of temperature on the PL spectra (right *y*-axis) and UV-vis absorption spectra (left *y*-axis) of CdS:Ag^+ doped-QDs synthesized at Q_A = 0.7 mL min^{-1}, Q_B = 0.2 mL min^{-1} and c_{TBP} = 0.067 mol L^{-1}. Due to the deep-site hetero-valence doping of Ag^+, the PL peak is located at 651 nm, corresponding to red fluorescence. When the temperature is increased from 40 °C to 60 °C, the fluorescence intensity of the QDs is gradually increased, and the fluorescence intensity is greatly improved with the increase in temperature. This is attributed to the fact that the increase in temperature is conducive to facilitating the reverse cation exchange reaction. From the perspective of the kinetic process, the increase in temperature speeds up the ion diffusion rate,

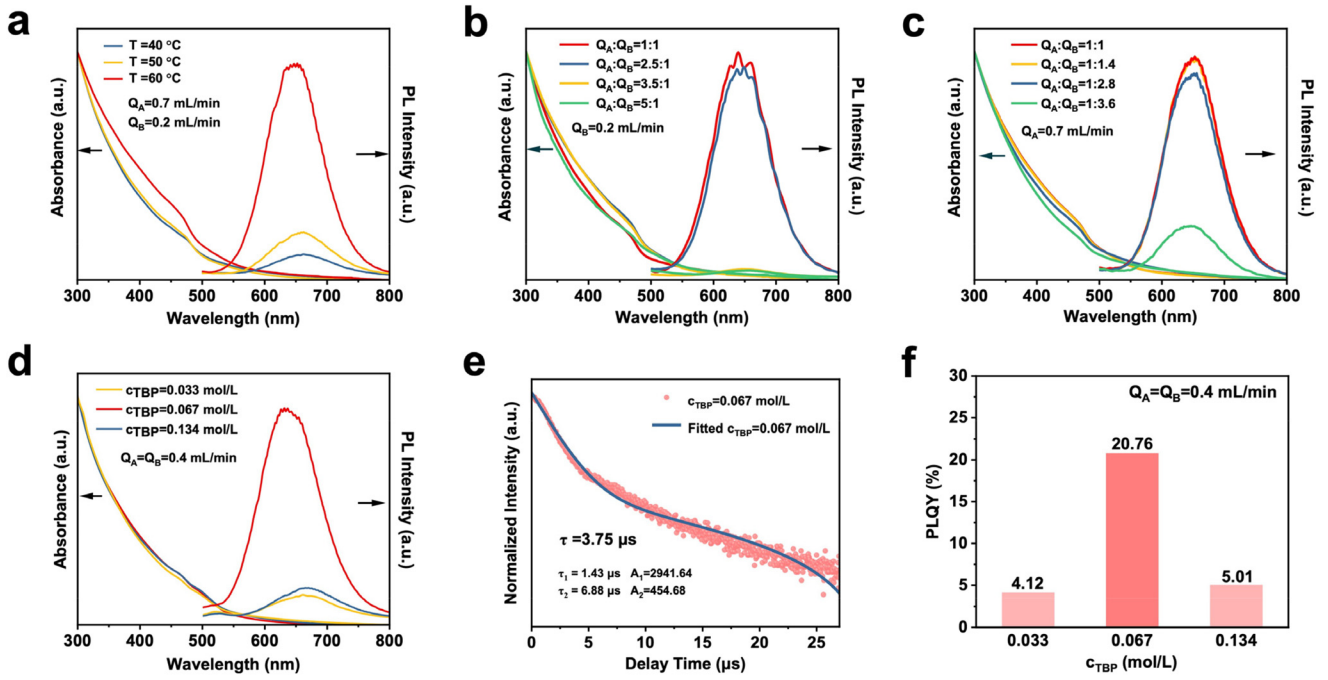

Fig. 3 (a) Effect of temperature on PL spectra and UV-vis absorption spectra of CdS:Ag^+ doped-QDs synthesized at a certain liquid flow rate and 0.067 mol L^{-1} TBP. (b) Effect of liquid flow rate of solution A on PL spectra and UV-vis absorption spectra of CdS:Ag^+ doped-QDs synthesized at 60 °C, 0.2 mL min^{-1} (Q_B) and 0.067 mol L^{-1} (c_{TBP}). (c) Effect of liquid flow rate of solution B on PL spectra and UV-vis absorption spectra of CdS:Ag^+ doped-QDs synthesized at 60 °C, 0.7 mL min^{-1} (Q_A) and 0.067 mol L^{-1} (c_{TBP}). (d) Effect of TBP concentrations on PL spectra and UV-vis absorption spectra of CdS:Ag^+ doped-QDs combined at 60 °C and 0.4 mL min^{-1} (Q_A = Q_B). (e) Fluorescence decay curve of CdS:Ag^+ doped-QDs tested at the optimal emission wavelength. (f) Photoluminescent quantum yields (PLQY) of CdS:Ag^+ doped-QDs synthesized at different TBP concentrations.

and the reaction process of Cd^{2+} replacing Ag^{+} is accelerated, which leads to faster synthesis of CdS:Ag^{+} doped-QDs. In the following research, the optimal reaction temperature was selected to be 60 °C.

In order to determine the influence of the flow rate ratio of the two solutions ($Q_A : Q_B$) on the luminescence performance of the QDs, the flow rate of the other solution was changed under the determined Q_A and Q_B respectively, and the absorption and PL spectra of the synthesized quantum dots were measured, as shown in Fig. 3b and c. Fig. 3b shows that at a low flow rate (Q_B = 0.2 mL min^{-1}), the fluorescence intensity decreases with the increase in the $Q_A : Q_B$. This is because when Q_B is determined, the increase in Q_A results in an increase in TBP. As previous studies have mentioned,[31,44] R_3P ligands (*e.g.*, TBP) could induce the reverse cation exchange reaction by mediating the thermodynamics of the reaction. An appropriate concentration of phosphine is necessary to modulate the composition and crystallinity of the products. Fig. 3c shows that a similar phenomenon also exists in the case of a larger flow rate (Q_B = 0.7 mL min^{-1}) and the fluorescence intensity decreases with the increase in $Q_A : Q_B$. Therefore, when the ratio of flow rate is 1 : 1, QDs with the highest fluorescence intensity are obtained. In the subsequent experiments, the ratio of the flow rate of the two solutions was set at 1 : 1.

To explore the effect of the concentration of TBP on the reaction, three TBP concentrations (0.033 mol L^{-1}, 0.067 mol L^{-1} and 0.134 mol L^{-1}) were selected for further investigation. Fig. 3d shows that under the condition of the same liquid flow rate and a reaction temperature of 60 °C, the luminous intensity reaches the highest value when the TBP concentration is 0.067 mol L^{-1}. Fig. 3e–f and Fig. S6a–d† show fluorescence lifetime and PLQY of CdS:Ag^{+} doped-QDs synthesized at different concentrations of TBP at a liquid flow rate of 0.4 mL min^{-1}. The fluorescence lifetime was fitted using a double exponential function:

$$I(t) = I_0 + A_1 \exp\left(-\frac{t}{t_1}\right) + A_2 \exp\left(-\frac{t}{t_2}\right) \quad (1)$$

The average lifetime (τ_0) is calculated using the following formula:

$$\tau_0 = \frac{A_1\tau_1^2 + A_2\tau_2^2}{A_1\tau_1 + A_2\tau_2} \quad (2)$$

where A_1 and A_2 are the weight factors of the two exponential attenuation components, τ_1 and τ_2 are the fluorescence lifetimes of the two exponential decay processes, and t represents the time elapsed from the beginning of excitation, used to describe the change in fluorescence attenuation over time. The results show that the fluorescence lifetimes of CdS:Ag^{+} doped-QDs under different synthesis conditions are on the timescale of microseconds, which proves that doped fluorescence is dominant in CdS:Ag^{+} doped-QDs. The long-lived red fluorescence further supports the advantage of the emission associated with Ag^{+} doping. Double exponential fitting was used to fit the data in the figure, and it was found that the difference in fluorescence lifetime was not significant. However, the PLQY of CdS:Ag^{+} doped-QDs synthesized at 0.067 mol L^{-1} was 4–5 times higher than that of QDs synthesized under other conditions, which further verified that the concentration of the phosphine ligand had a significant effect on the kinetics of the cation exchange reaction. As a result, 0.067 mol L^{-1} TBP is demonstrated to be the most suitable reaction concentration for the process of MPB.

After determining the liquid flow ratio and concentration of the reactants, varying internal particle sizes of 1.2 mm, 2.0 mm, 2.5 mm, and 3.0 mm were selected to investigate the reaction efficiency. The PL spectra of CdS:Ag^{+} doped-QDs synthesized under MPB with different internal particle sizes are shown in Fig. 4a. The PL intensity in the presence of MPB is higher than that without the mixing section, which further indicates that the presence of MPB is conducive to rapid and uniform mixing in the initial stage of the cation exchange reaction, and the PL intensity of CdS:Ag^{+} doped-QDs prepared by MPB with smaller particle sizes is higher. It could be concluded that MPB with smaller particle sizes can provide a larger effective interfacial area and promote the mixing degree of the two liquids, which could improve the uniformity and efficiency of the reaction. Fig. 4b shows that when the internal particle size is 1.2 mm and the liquid flow rate of the two liquids is 0.3 ml min^{-1}, the PLQY of the quantum dots prepared by the continuous method can reach 32.16%. As shown in Fig. 4c and d, there is no single linear relationship between fluorescence intensity and liquid flow rate. An excessively slow flow rate can result in localized accumulation of reactants, thereby reducing the uniformity of the product. Furthermore, the prolonged reaction time caused by a reduced flow rate may induce overreaction, which causes surficial defects on the QDs and ultimately degrades their fluorescence performance. In contrast, when the liquid flow rate is further increased, the residence time of the liquid in the reaction part is shortened, resulting in insufficient reaction and a decrease in fluorescence intensity. In general, the longer the length of the MPB, the better the mixing effect that can be achieved by virtue of the increased possibility of contact between the multiple reactants when passing through the MPB, thus achieving more complete mixing, which is beneficial for optimizing the photoelectric performance of CdS:Ag^{+} doped-QDs. Based on this, we chose to use a longer MPB of 18 cm. As shown in Fig. 4e, the photoluminescence intensity of CdS:Ag^{+} doped-QDs prepared by the lengthened MPB is improved. When the length of the MPB is 18 cm, the internal particle size is 2.0 mm, the flow rate of the two liquids is 0.2 ml min^{-1}, and the reaction temperature is 70 °C. The PLQY of the quantum dots prepared by using the MPB-intensified tube microreactor system can reach 50.8% (Fig. 4f), which is 10.8% higher than that for the products synthesized by the traditional batch flask method and 7.8% higher than the values produced by our previous microreactor platform.

Table 1 shows a comparison of CdS:Ag^{+} doped-QDs synthesized by different methods. CdS:Ag^{+} doped-QDs achieved a

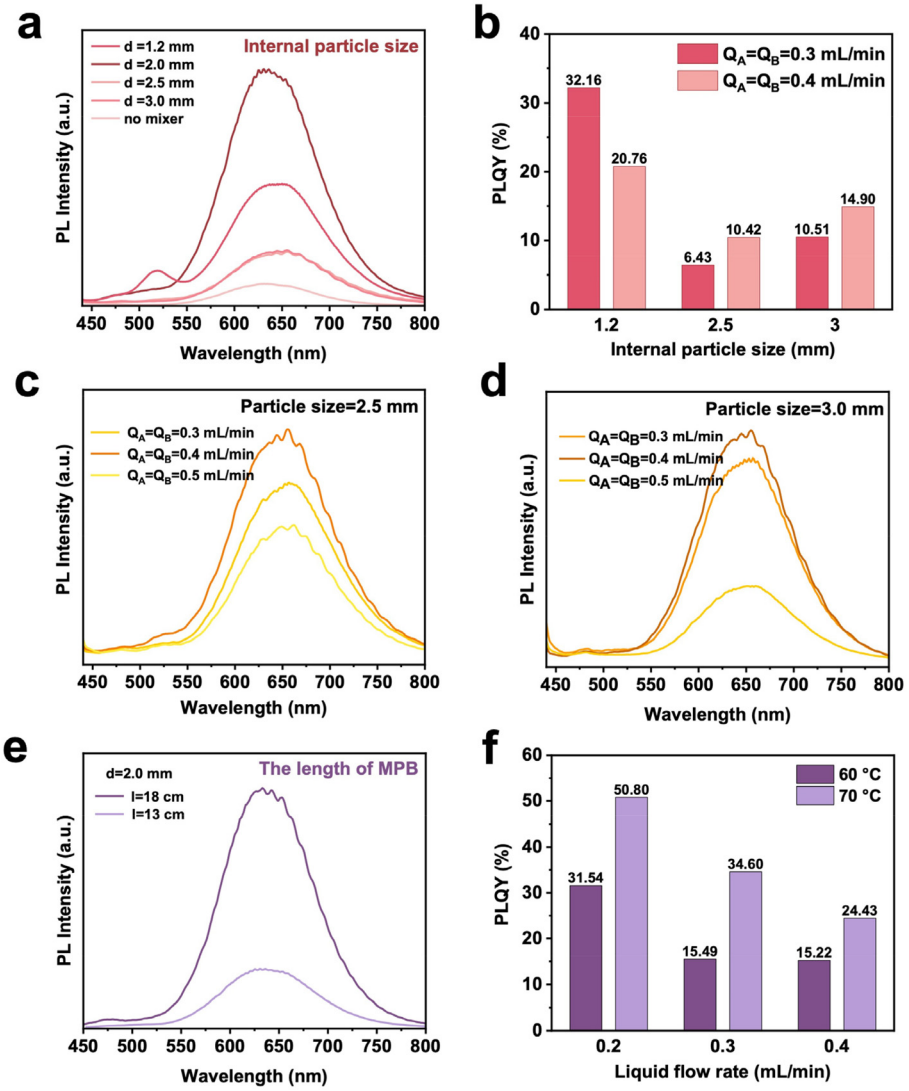

Fig. 4 (a) Effect of internal particle size on PL spectra of CdS:Ag^+ doped-QDs synthesized at Q_A = Q_B = 0.3 mL min^{-1}, 0.067 mol L^{-1} TBP, 60 °C and 13 cm of MPB. (b) Effect of internal particle size and liquid flow rate on the PLQY of CdS:Ag^+ doped-QDs synthesized at 0.067 mol L^{-1} TBP, 60 °C and 13 cm of MPB. (c) Effect of flow rate on PL spectra of CdS:Ag^+ doped-QDs synthesized at 2.5 mm particle size, 0.067 mol L^{-1} TBP, 60 °C and 13 cm of MPB. (d) Effect of flow rate on PL spectra of CdS:Ag^+ doped-QDs synthesized at 3.0 mm particle size, 0.067 mol L^{-1} TBP, 60 °C and 13 cm of MPB. (e) Effect of length of MPB on PL spectra of CdS:Ag^+ doped-QDs synthesized at 2.0 mm particle size, 0.067 mol L^{-1} TBP, 60 °C and Q_A = Q_B = 0.4 mL min^{-1}. (f) Effect of liquid flow rate and temperature on PLQY of CdS:Ag^+ doped-QDs synthesized at 0.067 mol L^{-1} TBP and 18 cm of MPB.

Table 1 Comparison of PLQY, yield, reaction time and the number of pumps of CdS:Ag^+ doped-QDs prepared by different methods

Method	PLQY	Yield	Reaction time	Flow rate	Number of pumps	PL peak	Ref.
Batch flask method	40.0%	43.01%	120 min	—	—	648 nm	29
Tube microreactor	43.0%	48.41%	60 min	40 μL min^{-1}	3	648 nm	41
MPB-intensified tube microreactor system	**50.8%**	**64.6%**	**30 min**	**0.2 mL min^{-1}**	**2**	**651 nm**	**This work**

PLQY of 50.8%, with the concomitant product yield reaching 64.6%, representing significant improvements over the traditional batch flask method and the tube microreactor method. The optimized system demonstrates 6-fold and 2.67-fold production increases over the two methods, respectively, while reducing the reaction duration to 30 minutes. Table 2 shows a comparison of different QDs prepared by the microreactor. From the perspective of process conditions, although the synthesis of CdS:Ag^+ doped-QDs in this work has advantages compared with previous synthesis methods, there is still

Table 2 Comparison of PLQY, yield, and reaction time of QDs prepared by different methods

Method	Types of QDs	PLQY	Reaction time	PL peak	Ref.
Microreactor	CdTe/ZnS QDs	23% ± 1%	20 min	598 nm ± 4 nm	45
Microreactor	Carbon dots	60.1%	1.66–5 min	455 nm	46
Microreactor	CdTe QDs	61.5%	—	500, 534, 570, 588, 630 nm	47
Microreactor	N-CQDs	84.1%	8 min	502–521 nm	48

room for optimization, such as using MPB to expand the synthesis of other types of QDs or further optimizing process parameters for more systematic and in-depth exploration.

The yield of CdS:Ag^+ QDs is calculated using the following formula:

$$y = \left(\frac{m_{\text{a-CdS}}}{m_{\text{t-CdS}}}\right) \times 100\% \quad (3)$$

where y is defined as the percentage of the actual obtained product mass ($m_{\text{a-CdS}}$) to the theoretically maximum possible product mass ($m_{\text{t-CdS}}$). The theoretical yield is calculated based on the complete conversion of the precursor Ag_2S in the reverse cation exchange reaction. In theory, the precursor Ag_2S (Ag_2S QDs) is completely converted into CdS, and according to the reaction metrology relationship ($Ag_2S + Cd^{2+} \rightarrow CdS + 2Ag^+$), the mole ratio of Ag_2S to CdS is 1 : 1. The theoretical CdS mass is

$$m_{\text{t-CdS}} = \left(\frac{m_{Ag_2S}}{M_{Ag_2S}}\right) \times M_{\text{CdS}} \quad (4)$$

where m_{Ag_2S} represents the initial mass of the Ag_2S precursor, M_{Ag_2S} represents the molar mass of Ag_2S and M_{CdS} represents the molar mass of CdS.

Conclusions

This study presents the development of a continuous flow synthesis platform utilizing a micropacked bed (MPB) intensified tube microreactor for the production of CdS:Ag^+ doped-QDs. By optimizing critical process parameters, including MPB configuration (18 cm length, 2.0 mm glass beads), flow rate (0.2 mL min^{-1}), and thermal conditions (70 °C), CdS:Ag^+ doped-QDs achieved a PLQY of 50.8% with a concomitant product yield reaching 64.6%. These performance metrics demonstrate substantial improvements over conventional batch flask (40% PLQY, 43.01% yield) and microreactor (43% PLQY, 48.41% yield) methodologies. The developed MPB system demonstrates multiple operational advantages: reaction duration reduced to 30 minutes, simplified fluidic architecture requiring only two pumps (*vs.* three in the microreactor system), and enhanced flow rate (0.2 mL min^{-1} *vs.* 40 μL min^{-1}). Production capacity analysis revealed 6-fold and 2.67-fold output increases compared to the conventional batch and microreactor systems, respectively, further showcasing the method's superior speed. These improvements highlight the strength of the MPB system in balancing rapid mass/heat transfer with precise control over cation exchange kinetics, addressing critical limitations of traditional synthesis approaches. Future research could explore the scalability of the MPB-intensified system for industrial applications by validating reactor stability under high-throughput conditions and integrating automation protocols.

Data availability

All relevant data are within the manuscript and the ESI.†

Further clarification of the data is available upon request from the authors.

Conflicts of interest

The authors declare no conflict of interest.

Acknowledgements

We gratefully acknowledge the support of the National Natural Science Foundation of China (52272186, 22378020, and 22375020), the Beijing Institute of Technology Research Fund Program for Young Scholars and the Analysis & Testing Center for this work.

References

1 Y. Wang, Q. Zhao, R. Haag and C. Wu, *Angew. Chem., Int. Ed.*, 2022, **61**, e202213974.
2 Y. Li, J. He, G. Lu, C. Wang, M. Fu, J. Deng, F. Yang, D. Jiang, X. Chen, Z. Yu, Y. Liu, C. Yu and Y. Cui, *Nat. Commun.*, 2024, **15**, 7044.
3 S. Tomasi Masoni, M. Antognoli, A. Mariotti, R. Mauri, M. V. Salvetti, C. Galletti and E. Brunazzi, *Chem. Eng. J.*, 2022, **437**, 135113.
4 H. Yang, G. Yao and D. Wen, *Chem. Eng. Sci.*, 2021, **235**, 116368.
5 M. Atobe, H. Tateno and Y. Matsumura, *Chem. Rev.*, 2018, **118**, 4541–4572.
6 J. Ran, X. Wang, Y. Liu, S. Yin, S. Li and L. Zhang, *Mater. Horiz.*, 2023, **10**, 2343–2372.
7 L. Sang, T. Zhou, W.-Y. Yang, Y. Cai, H.-D. Zhang and Y. Lang, *Chem. Eng. Sci.*, 2025, **307**, 121342.

8 Y. Fan, P. Wang, J. Zhang, M. Huang, W. Liu, Y. Xu, X. Duan, Y. Li and J. Zhang, *Chem. Eng. J.*, 2024, **484**, 149404.
9 W. Lai, C. Wu and X. Han, *Chem. Eng. J.*, 2023, **451**, 138383.
10 J. H. Bannock, M. Al-Hashimi, S. H. Krishnadasan, J. J. M. Halls, M. Heeney and J. C. de Mello, *Mater. Horiz.*, 2014, **1**, 214–218.
11 K. S. Elvira, X. C. I Solvas, R. C. R. Wootton and A. J. deMello, *Nat. Chem.*, 2013, **5**, 905–915.
12 A. M. Nightingale, S. H. Krishnadasan, D. Berhanu, X. Niu, C. Drury, R. McIntyre, E. Valsami-Jones and J. C. deMello, *Lab Chip*, 2011, **11**, 1221–1227.
13 Y. Bian, X. Yan, F. Chen, Q. Li, B. Li, W. Hou, Z. Lu, S. Wang, H. Zhang, W. Zhang, D. Zhang, A. Tang, F. Fan and H. Shen, *Nature*, 2024, **635**, 854–859.
14 X. Lin, Y. Yang, X. Li, Y. Lv, Z. Wang, J. Du, X. Luo, D. Zhou, C. Xiao and K. Wu, *Nat. Nanotechnol.*, 2024, **20**, 229–236.
15 G. S. Selopal, H. Zhao, Z. M. Wang and F. Rosei, *Adv. Funct. Mater.*, 2020, **30**, 2070086.
16 M. L. Zaffalon, V. Pinchetti, A. Camellini, S. Vikulov, C. Capitani, B. Bai, M. Xu, F. Meinardi, J. Zhang, L. Manna, M. Zavelani-Rossi, S. A. Crooker and S. Brovelli, *Energy Mater. Adv.*, 2021, **2021**, 1959321.
17 M. Abdullah Issa, Z. Z. Abidin, S. Sobri, S. Rashid, M. Adzir Mahdi, N. Azowa Ibrahim and M. Y. Pudza, *Nanomaterials*, 2019, **9**, 1500.
18 M. Yahaya Pudza, Z. Zainal Abidin, S. Abdul Rashid, F. Md Yasin, A. S. M. Noor and M. A. Issa, *Nanomaterials*, 2020, **10**, 315.
19 H. Yang, L. Gutiérrez-Arzaluz, P. Maity, M. A. Abdulhamid, J. Yin, Y. Zhou, C. Chen, Y. Han, G. Szekely, O. M. Bakr and O. F. Mohammed, *Energy Mater. Adv.*, 2021, **2021**, 9873846.
20 Y. E. Panfil, M. Oded and U. Banin, *Angew. Chem., Int. Ed.*, 2018, **57**, 4274–4295.
21 G. Rainò, M. A. Becker, M. I. Bodnarchuk, R. F. Mahrt, M. V. Kovalenko and T. Stöferle, *Nature*, 2018, **563**, 671–675.
22 H. Moon, C. Lee, W. Lee, J. Kim and H. Chae, *Adv. Mater.*, 2019, **31**, 1804294.
23 S. Bao, H. Yu, G. Gao, H. Zhu, D. Wang, P. Zhu and G. Wang, *Nano Res.*, 2022, **15**, 3594–3605.
24 Y. Yang, Y. Xie and F. Zhang, *Adv. Drug Delivery Rev.*, 2023, **193**, 114697.
25 C. Ding, Y. Huang, Z. Shen and X. Chen, *Adv. Mater.*, 2021, **33**, 2007768.
26 H. Yang, H. Huang, X. Ma, Y. Zhang, X. Yang, M. Yu, Z. Sun, C. Li, F. Wu and Q. Wang, *Adv. Mater.*, 2021, **33**, 2103953.
27 M. Yahaya Pudza, Z. Zainal Abidin, S. Abdul Rashid, F. Md Yasin, A. S. M. Noor and M. A. Issa, *Processes*, 2019, **7**, 704.
28 M. Y. Pudza, Z. Z. Abidin, S. Abdul-Rashid, F. M. Yassin, A. S. M. Noor and M. Abdullah, *ChemistrySelect*, 2019, **4**, 4140–4146.
29 J. Gui, M. Ji, J. Liu, M. Xu, J. Zhang and H. Zhu, *Angew. Chem., Int. Ed.*, 2015, **54**, 3683–3687.
30 B. Bai, C. Zhao, M. Xu, J. Ma, Y. Du, H. Chen, J. Liu, J. Liu, H. Rong, W. Chen, Y. Weng, S. Brovelli and J. Zhang, *Chem*, 2020, **6**, 3086–3099.
31 L. De Trizio and L. Manna, *Chem. Rev.*, 2016, **116**, 10852–10887.
32 X. Peng, *Adv. Mater.*, 2003, **15**, 459–463.
33 L. Zhang, H. Yang, Y. Tang, W. Xiang, C. Wang, T. Xu, X. Wang, M. Xiao and J. Zhang, *Chem. Eng. J.*, 2022, **428**, 131159.
34 L. Gu, J. Zhang, G. Yang, Y. Tang, X. Zhang, X. Huang, W. Zhai, E. K. Fodjo and C. Kong, *Food Chem.*, 2022, **376**, 131898.
35 Y. Liu, X. Chen and Q. Ma, *New J. Chem.*, 2018, **42**, 4102–4108.
36 R. Xu, C. Qiao, M. Xia, B. Bai, Y. Li, J. Liu, J. Liu, H. Rong, M. Xu and J. Zhang, *J. Mater. Chem. C*, 2021, **9**, 7194–7199.
37 W. Huang, M. Xu, J. Liu, J. Wang, Y. Zhu, J. Liu, H. Rong and J. Zhang, *Adv. Funct. Mater.*, 2019, **29**, 1808762.
38 C. Li, J. Li, L. Ji, Y. Zhu, J. Liu and J. Zhang, *Nano Res.*, 2024, **17**, 10467–10475.
39 J. S. Santana and S. E. Skrabalak, *Adv. Energy Mater.*, 2020, **10**, 1902051.
40 Y. Chen, A. Shen, J. Guo, L. Zhu, G. Li, Y. Qin, X. Qu, C.-F. Wang and S. Chen, *Chem. Eng. J.*, 2023, **471**, 144444.
41 Y. Li, Y. Li, X. Li, T. Hou, C. Qiao, Y. Tai, X. Gu, D. Zhao, L. Sang and J. Zhang, *Nano Res.*, 2022, **15**, 9647–9653.
42 L. Li, F. Hu, D. Y. Xu, S. L. Shen and Q. B. Wang, *Chem. Commun.*, 2012, **48**, 4728–4730.
43 Q. Di, J. Wang, Z. Zhao, J. Liu, M. Xu, J. Liu, H. Rong, W. Chen and J. Zhang, *Chem. – Eur. J.*, 2018, **24**, 18643–18647.
44 J. Liu and J. Zhang, *Chem. Rev.*, 2020, **120**, 2123–2170.
45 R. Kikkeri, P. Laurino, A. Odedra and P. H. Seeberger, *Angew. Chem., Int. Ed.*, 2010, **49**, 2054–2057.
46 L. Rao, Y. Tang, Z. Li, X. Ding, G. Liang, H. Lu, C. Yan, K. Tang and B. Yu, *Mater. Sci. Eng., C*, 2017, **81**, 213–223.
47 S. Pandey, D. Mukherjee, P. Kshirsagar, C. Patra and D. Bodas, *Mater. Today Bio*, 2021, **11**, 100123.
48 Y. Tang, L. Rao, Z. Li, H. Lu, C. Yan, S. Yu, X. Ding and B. Yu, *Sens. Actuators, B*, 2018, **258**, 637–647.